J Supercond Nov Magn (2012) 25:2557–2565
DOI 10.1007/s10948-012-1767-y

LETTER

Results of Measuring the Influence of Casimir Energy on Superconducting Phase Transitions

Annalisa Allocca · Giuseppe Bimonte · Detlef Born · Enrico Calloni · Giampiero Esposito · Uwe Huebner · Evgeni Il'ichev · Luigi Rosa · Francesco Tafuri

Received: 28 August 2012 / Accepted: 31 August 2012 / Published online: 18 September 2012

Abstract The ALADIN experiment aims at observing how the critical magnetic field of a superconducting aluminum film is modified, when it constitutes one of the reflecting surfaces of a Casimir cavity. If successful, such an observation would reveal the influence of vacuum energy on the superconducting phase transition. In this paper, a rigorous analysis of experimental data is reported, the results are discussed and compared with theoretical predictions based on Lifshitz theory of dispersion forces, and the BCS formula for the optical conductivity of superconductors. Thanks to this rigorous analysis, it can now be asserted that in the region of energy where it is expected that Casimir energy is comparable with condensation energy and the deviations of critical field from BCS formula to be not negligible, an anomalous behavior is found.

Keywords Casimir effect · Superconductors · Critical field

A. Allocca
Dipartimento di Fisica, Università di Siena, via Roma 56, 53100 Siena, Italy

A. Allocca
INFN, sezione di Pisa, Largo Pontecorvo 3, Polo Fibonacci Edificio C, 56127 Pisa, Italy

G. Bimonte · E. Calloni · L. Rosa
Dipartimento di Scienze Fisiche, Università Federico II, Complesso Universitario di Monte S. Angelo, Via Cintia, Edificio 6, 80126 Napoli, Italy

G. Bimonte · E. Calloni (✉) · G. Esposito · L. Rosa
INFN, Sezione di Napoli, Complesso Universitario di Monte S. Angelo, Via Cintia, Edificio 6, 80126 Napoli, Italy
e-mail: enrico.calloni@na.infn.it

D. Born · U. Huebner · E. Il'ichev
Institute for Photonic Technology, Postfach 10 02 39, 07702 Jena, Germany

D. Born · F. Tafuri
Dipartimento di Ingegneria dell'Informazione, Seconda Università degli Studi di Napoli, via Roma 29, 81031 Aversa Ce, Italy

1 Introduction

The Casimir effect [1, 2] provides a striking manifestation of vacuum quantum fluctuations of the electromagnetic field in bounded geometries, and it represents a rare example of a purely quantum phenomenon that can be tested at the mesoscopic scale. The Casimir effect has received much attention over the past decades thanks to a wave of new experiments which made it possible to measure the Casimir force with unprecedented precision. For a recent review of these experiments and a critical survey of the numerous theoretical investigations on the Casimir effect in materials, we address the reader to the recent monograph [3], and also to the work in [4, 5].

Despite the impressive theoretical and experimental advances made over the past 20 years, the Casimir effect still faces important unsolved questions at the fundamental level, in particular the problem of reconciling the vacuum energy density and its interaction with the gravitational field, known as the cosmological constant problem [6, 7]. No experimental verification that vacuum fluctuations gravitate according to the equivalence principle has been obtained so far, even though there are theoretical expectations that this should be the case [8–16]. Relying upon these considerations, some of us studied the effect of a gravitational field on a rigid Casimir cavity, by computing the net force acting on it: interestingly, it was found that a Casimir apparatus, when subject

to the weak gravitational field of the Earth, should experience a tiny push in the upward direction [17–22]. In [17–19], it was argued that an experimental verification of this effect is extremely hard, if not impossible, under static conditions, by virtue of the extreme smallness of the expected force. A better possibility would be to carry out the measurement dynamically, i.e., by modulating the Casimir energy stored in a rigid cavity in a known way. Such a modulation of the Casimir energy might be achieved by altering periodically the reflectivity of the plates. Recently, a significant modulation of the Casimir force between a highly doped semiconducting membrane and a gold plate has been demonstrated experimentally [23, 24], by shining periodic laser pulses on the membrane which determine a large change in the charge carrier density of the membrane. Despite being interesting for Casimir studies, this result is not suitable for "weighting" aims: The energy supplied to the system to induce the change in carrier density is many orders of magnitude larger than the variation of Casimir energy. This would make it extremely difficult to observe the tiny fraction of mass change due to the Casimir contribution. On the contrary, in our scheme based on the superconducting phase transition, the total change of energy is of the same order of magnitude as the change in the Casimir energy and, therefore, its contribution might in principle be observed.

This is the framework of the ALADIN experiment, whose aim is to observe the variation of the Casimir energy stored in a superconducting Casimir cavity, constituted by a thin superconducting film separated by a thin oxide layer from a thick gold substrate, across the superconducting phase transition. The scheme of detection is based on a measurement of the critical magnetic field that destroys the superconductivity of the film, whose magnitude is expected to be affected by the Casimir energy. If successful, the experiment would thus reveal the influence of vacuum energy on a phase transition. Another distinctive feature of our setup is that we use rigid cavities that are obtained by deposition techniques, a feature which might be useful to investigate experimentally the dependence of the Casimir energy on the geometrical shape of the intervening bodies, an issue that remains under scientific debate also at a theoretical level [3].

The plan of the paper is a follows: In Sect. 2, we briefly describe the experimental setup and the measurement method, and Sect. 3 is devoted to the analysis method based on cross-correlation. Finally, the experimental results are discussed in Sect. 4. Indeed, a preliminary analysis of the data reported in this paper had already been performed some time ago as described in a Conference Proceedings paper, where "*the sensitivity had been roughly estimated*" [25].

The analysis reported in this paper, based on a procedure of cross-correlation, is instead rigorous and the results are now better estimated and make it possible to develop a deeper discussion.

2 ALADIN: Experimental Setup and Expected Effect

Before we describe our experimental setup, it is useful to briefly recall the principle at the basis of our experiment that was described in detail in the works [40, 41]. The starting observation is that, according to Lifshitz theory [3], the Casimir energy is determined by the optical properties of the plates. Since the optical properties of a superconductor are sharply different from those of a normal metal [42], one is led to expect that the Casimir free energy $F^{(C)}$ stored in a superconducting cavity should change across the superconducting transition. The change $\Delta F^{(C)} = F_n^{(C)} - F_s^{(C)}$ of Casimir energy was estimated in [40, 41] (see also [43, 44]), on the basis of Lifshitz theory by using the BCS formula for the optical conductivity of superconductors, and it was found to be extremely small. This is not surprising of course, because the superconducting transition alters the optical properties of a metal only in the microwave region, which constitutes a small window in the wide frequency range that contributes to the Casimir energy. The latter typically extends up to a few times the characteristic cavity frequency $\omega_c = c/2d$, with d the plate separation, which for typical submicron separations belongs to the infrared region of the spectrum. The smallness of the fractional change of Casimir energy across the superconducting transition makes it impossible to observe the corresponding change in the Casimir force on the plates, with present day sensitivities in force measurements.

The Aladin experiment uses a detection scheme which does not involve at all a force measurement, as it aims at observing how the variation $\Delta F^{(C)}$ of Casimir energy affects the critical magnetic field H_c of a thin superconducting film which is part of a Casimir cavity. To see how this comes about, we recall [45] that the magnitude of the parallel critical field H_c for a thick superconducting slab of volume V can be determined by equating the magnetic work $V H_c^2/8\pi$ required to expel the magnetic field from the sample, with the so-called condensation energy $\varepsilon_{\rm cond}(T)$ of the material, which represents the difference of Helmholtz free energies between the normal and the superconducting phases:

$$V\frac{H_c^2(T)}{8\pi} = \varepsilon_{\rm cond}(T). \tag{1}$$

When the film is one of the two plates of a Casimir cavity, we have to augment the right-hand side of the above equation by the difference $\Delta F^{(C)}$ between the Casimir energies in the normal and in the superconducting phases:

$$V\frac{H_c^2(T)}{8\pi} = \varepsilon_{\rm cond}(T) + \Delta F^{(C)}(T). \tag{2}$$

In writing this relation, we are tacitly assuming that the fluctuating electromagnetic field in the Casimir cavity does not alter significantly the properties of the superconductor,

and in particular its condensation energy. This may be considered as a plausible assumption, as far as $\Delta F^{(C)}(T) \ll \varepsilon_{\rm cond}(T)$. According to Eq. (2), the variation $\Delta F^{(C)}(T)$ of Casimir energy determines a change in the magnitude of the critical field $H_{\rm c}$, which for $\Delta F^{(C)}(T) \ll \varepsilon_{\rm cond}(T)$ is estimated to be

$$\frac{\delta H_{\rm c}}{H_{\rm c}} \approx \frac{\Delta F^{(C)}(T)}{2\,\varepsilon_{\rm cond}(T)}. \tag{3}$$

The key thing to notice is that the condensation energy of a thin superconducting film can easily be orders of magnitudes smaller than typical Casimir energies $F_n^{(C)}$ and, therefore, one may hope that even tiny fractional changes of Casimir energy $\Delta F^{(C)}(T)$ can determine observable shifts of the critical field. For example, for a Beryllium film, we estimated [40, 41] that a relative variation of $F^{(C)}$ of one part over 10^8 might lead to a 5 percent variation of critical magnetic field.

Detailed numerical computations [41] show that the magnitude of the effect increases for thin films, because they have a smaller condensation energy, and for small cavity widths d, because the change of Casimir energy becomes larger. It is important to remark that the relative shift of critical field was found to be roughly proportional to the inverse of the transition temperature $T_{\rm c}$ of the superconducting material. The main reason why superconductors with low $T_{\rm c}$ lead to a larger effect is that the condensation energy is empirically known to scale as $T_{\rm c}^{2.6}$ [46], and this makes the denominator in the r.h.s. of Eq. (3) decrease faster than the numerator as $T_{\rm c}$ decreases. As a compromise between the possibility to perform preliminary tests, easy change of structures, statistics and signal-to-noise ratio, we chose to work around 1.5 K, using Al as superconducting material. Besides having a low critical temperature, Al is a material that oxides easily, and this makes it easier to grow oxide layers of controllable thicknesses, well attached to the superconducting film, that constitute the dielectric medium of our metallic Casimir cavities. The configuration used in the experiment is a three-layer cavity, made of a thin superconducting Al film ($5 \div 10$ nm), a thin dielectric layer of native oxide (Al_2O_3)($5 \div 10$ nm), and a thick metallic layer of Au (100 nm). However, at present, we are considering different configurations in order to obtain a larger signal-to-noise ratio in the expected effect.

In our experiment, we used a cryogenic system based on the Heliox VL ^{3}He cryostat, inserted into a dewar equipped with magnetic screening, which isolates the samples from external EM fields. Since it is extremely difficult to keep the cryostat temperature perfectly constant, we did not try to measure the critical field $H_{\rm c}$ of the samples as a function of the temperature. Rather, we measure how the critical temperature $T_{\rm c}(H)$ of the samples *changes* as a function of the applied magnetic field H. More precisely, for each value of the applied field H, we measure the relative *shift*

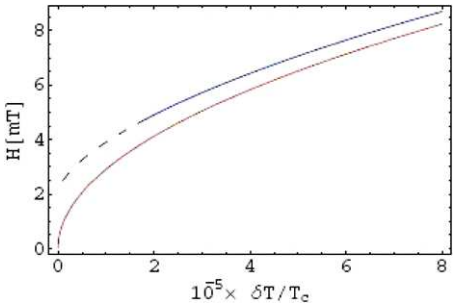

Fig. 1 Simulation of the expected signal for a bare thin Al film of thickness $D = 14$ nm (*lower curve*) and for a cavity consisting of a similar Al film, covered by a 6 nm dielectric layer and a 100 nm Au mirror (*upper curve*)

$\delta t = (T_{\rm c}(H) - T_{\rm c0})/T_{\rm c0}$ in the critical temperature $T_{\rm c}$ of the sample, with respect to the critical temperature T_{c0} of the same sample in zero field. As we shall explain below, by using the method of *cross-correlations*, the shift δt can be measured much more accurately than the individual critical temperatures in the applied and in the null fields. Our theory predicts (see Fig. 1 and comments below) that the curve $H(\delta t)$ for the bare film should lie below that for the film in the Casimir cavity. Since this is a *differential* measurement, we need a very good sensitivity in temperature, of order a few μK in the case of Al. As described in [25], the critical temperature is determined by measuring the resistance of a sample $R(T)$ in a four-wire configuration around the phase transition, for different external applied fields. For further details on the experimental set-up and the ultimate resolution achieved for different kinds of measurements performed in the same cryostat can be found in [26–39]. Several measurements have been performed and different samples have been tested, so as to find the best experimental conditions for a good signal-to-noise ratio. For a good data analysis to be possible, it was important to make sure that the transition curves did not change their profiles in time, or after applying a magnetic field. By employing these criteria, the best samples have been selected. Data reported in the following were obtained from the samples showing the sharper transition and the highest homogeneity among transition curves. For a detailed description of sample preparation, cryogenic apparatus, and measurement scheme, see [25].

The expected effect is shown in Fig. 1. Here, the critical magnetic field H is plotted against the shift $\delta t = 1 - t$ of the *reduced* critical temperature $t = T_{\rm c}(H)/T_{\rm c0}$ (with $T_{\rm c0}$ zero-field transition temperature). We recall [45] that for a (bare) thin superconducting film, with a thickness D much less than the penetration length λ, incomplete field expulsion leads to higher values of the parallel critical field H, as compared to bulk samples. For $1 - t \ll 1$ (as in our case),

the thin-film critical magnetic field H follows the simple law [45]

$$H = H_0\sqrt{24}\frac{\lambda(0)}{D}\sqrt{1-t}, \tag{4}$$

where $\lambda(0)$ is the penetration depth and H_0 is the bulk critical field, both determined for zero temperature.

For the in-cavity film, we can divide the expected signal curve (upper curve in Fig. 1) into three temperature regions. For temperatures far from the transition temperature of the film (region not shown in Fig. 1), the in-cavity curve coincides with the bare film curve, since the vacuum energy contribution becomes negligible compared to the condensation energy. When $\delta t \approx 3 \times 10^{-5}$, the change of Casimir energy is small but no longer negligible, and a perturbative approach is possible in $\delta H/H$: for $H \approx 5 \div 6$ mT; the two curves are expected to differ by an amount $\delta t \approx 6 \times 10^{-6}$. Note that, since the critical temperature of Al is 1.5 K, this corresponds to a shift in temperature of order 10 μK. Finally, for lower temperatures the dependence of δt on H for the in-cavity curve is expected to differ from the bare film case, because the Casimir energy contribution is of the same order of magnitude as the condensation energy. In this region, we are not able to perform any perturbative calculation, and there is no theoretical prediction for the curve's trend (dashed line in Fig. 1).

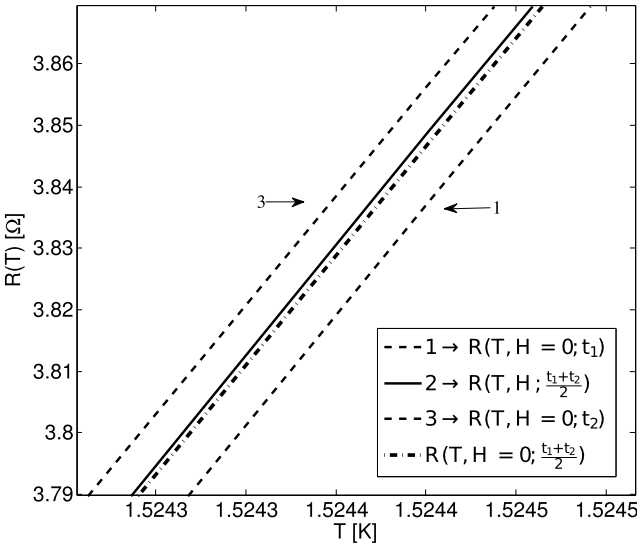

Fig. 2 Example of the measurement sequence. All measurements are performed at equal time intervals. Before and after each measurement with the applied field, a measurement in the absence of field is performed. From the two measurements in the absence of the field, it is possible to reconstruct the zero-field curve that would be measured simultaneously to the transition curve in the presence of the magnetic field. ΔT_c is the distance in temperature between the $R(T)$ curve in the presence of the magnetic field (*continuous line*), and the reconstructed $R(T)$ curve in zero field (*dashed-dotted line*)

3 Analysis Method Based on Cross-Correlation

As was explained in the previous section, for each value of the applied magnetic field H, we need to determine accurately the fractional shift δt of the critical temperature of the sample, relative to its critical temperature T_{c0} in zero field. As described in [25], the major source of noise in our measurements is the electronic noise at the read-out amplifier. This noise has a "fast" component (with time scale of one second) that determines a statistical error of a few μK, and a slow thermal drift (linear in time, about 50 μK per hour) that produces a shift proportional to the time elapsed between two measurements. To correct for the thermal drift, we arranged our measurements in series of triplets, as is shown in Fig. 2. Each triplet consists of three measurements of the curve $R(T)$ that are equally spaced in time, the first and the last one of which (left-most and right-most dashed curves in Fig. 2) are performed in zero-field, while the intermediate one (continuous line in Fig. 2) is done with the field applied. Since the slow thermal drift is linear in time, and since the two zero-field measurements are performed at equal time intervals before and after the applied field measurement, it is possible to "reconstruct" out of them the position that the zero-field curve $R(T)$ would have occupied in the R–T plane (dotted-dashed line in Fig. 2), had it been measured at the same time as the applied field curve. The relative shift δt in the critical temperatures is then determined by comparing the measured curve $R(T)$ in the applied field, with the reconstructed curve in zero field. Having explained the general scheme of the measurements, let us see how the method of cross-correlations permits to accurately determine δt.

The key feature of the $R(T)$ curves that allows to use the cross-correlation method to accurately determine the shifts δt is that, for each sample, their *shape* is practically independent of both the intensity of the applied magnetic field, and the time at which the measurements are performed. In other words, the curves $R(T)$ that are taken at different times, or in different fields, appear to differ from each other just by some horizontal translation Δ along the temperature axis. The cross-correlation method is ideally well suited to determine the amount of this translation, independently of any model for the shape of the curves. The idea is very simple, and consists in looking for the translation that *maximizes* the *overlap* between any two $R(T)$ curves. Let us see how this works out in detail. In reality, each $R(T)$ curve consists of a large number of data points more or less scattered in the T–R plane, around some ideal transition curve. We consider only data points that belong to the transition region, having a width of a few mK, around the critical temperature. Typically, this region contains a few thousand points for each curve. At this point, we cover the T–R plane by a rectangular grid whose axes are parallel to the T and R coordinate axis, and whose steps are s_T and s_R, respectively. The

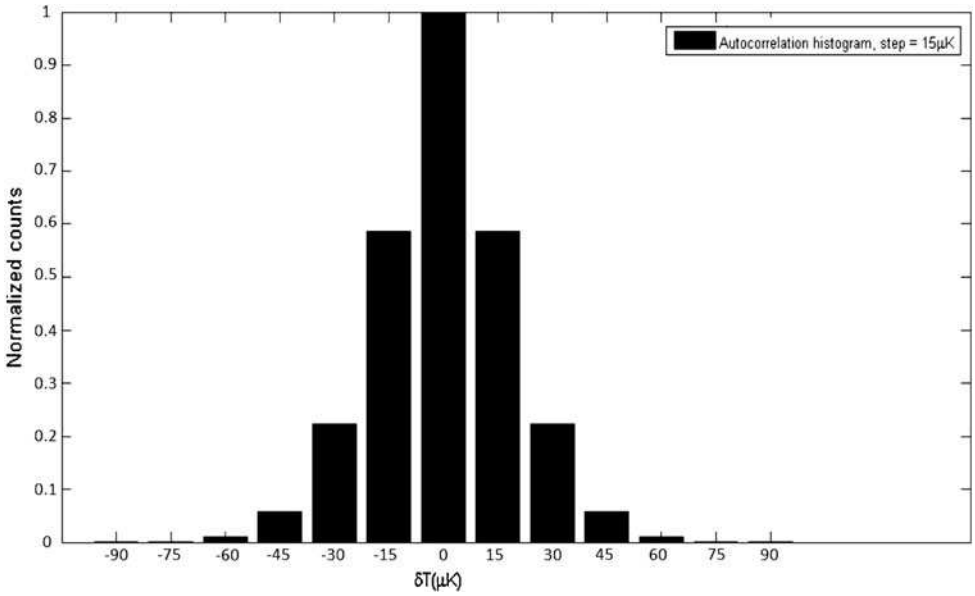

Fig. 3 Self-correlation of the $R(T)$ curve obtained with a lattice step on the abscissa equal to 15 μK

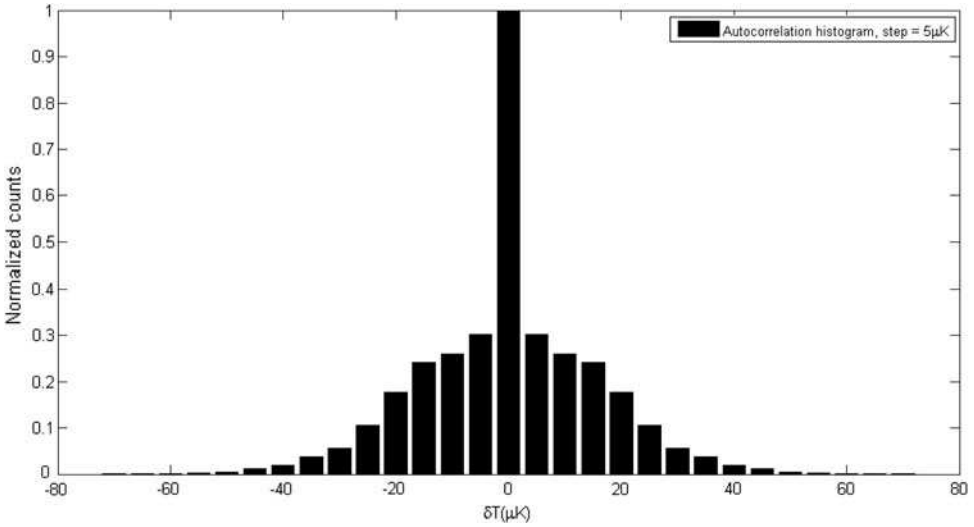

Fig. 4 Self-correlation of the $R(T)$ curve with lattice step equal to 5 μK

points $p_{i,j}$ of the grid in the T–R plane thus have coordinates $\{i\, s_T + a_t, j\, s_R + a_R\}$, where $\{a_T, a_R\}$ are the coordinates of the grid's origin. We let $\mathcal{H}_{i,j}$ be the number of data points that occupy the grid cell whose left-down corner coincides with the point $p(i, j)$ of the grid. Clearly, the number of points occupying the non-empty cells depends on the size of the cells, i.e., on the steps s_T and s_R. We shall discuss below the criterion we used to choose these steps. In practice, for the chosen size of the steps, the occupied cells turn out to include about five or six data points. Consider now any two transition curves $R^{(a)}(T)$ and $R^{(b)}(T)$ (not necessarily distinct), and let $\mathcal{H}^{(a)}_{i,j}$ and $\mathcal{H}^{(b)}_{i,j}$ be the respective histograms. For any translation of $R^{(b)}(T)$ by n steps along the T-axis, we define the cross-correlation $\mathcal{C}^{(a,b)}[n]$, to be the quantity

$$\mathcal{C}^{(a,b)}[n] = \sum_{i,j} \mathcal{H}^{(a)}_{i,j}\, \mathcal{H}^{(b)}_{i-n,j}. \tag{5}$$

The quantity $C^{(a)}[n] \equiv C^{(a,a)}[n]$ shall be denoted in what follows as the self-correlation of the curve $R^{(a)}(T)$. Intuitively, $\mathcal{C}^{(a,b)}[n]$ measures how well $R^{(a)}(T)$ and $R^{(b)}(T)$ overlap, after we translate $R^{(b)}(T)$ by an amount $n \times s_T$ along the T-axis.

In Figs. 3 and 4, we plot the normalized self-correlation $\mathcal{C}[n]$ of one of our $R(T)$ curves, for two different steps s_T. In Fig. 5, we plot the self-correlations and the crossed correlations of two of our curves, one measured in zero field and the other in a nonzero field. We verified that all correlations have a Gaussian shape around the central peak. More importantly, we see from Fig. 5 that the maximum of the cross-correlation between the zero-field curve and the nonzero-field curve is of the same order of magnitude as the maximum of the self-correlations of the two curves. From this circumstance, we infer that the two curves actually have equal

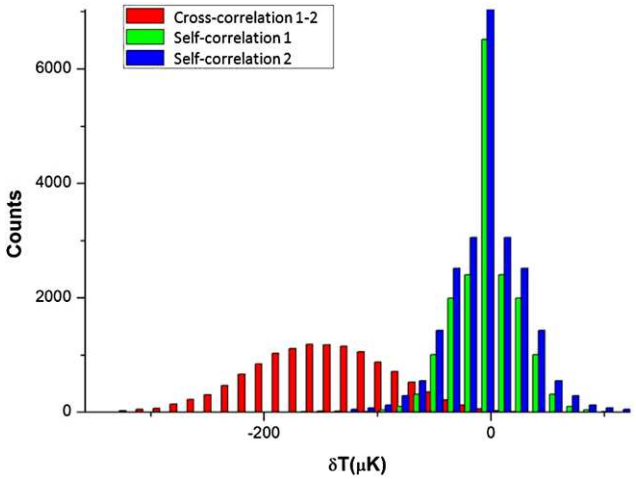

Fig. 5 Self-correlation of two $R(T)$ curves, green and blue, and cross–correlation among the two

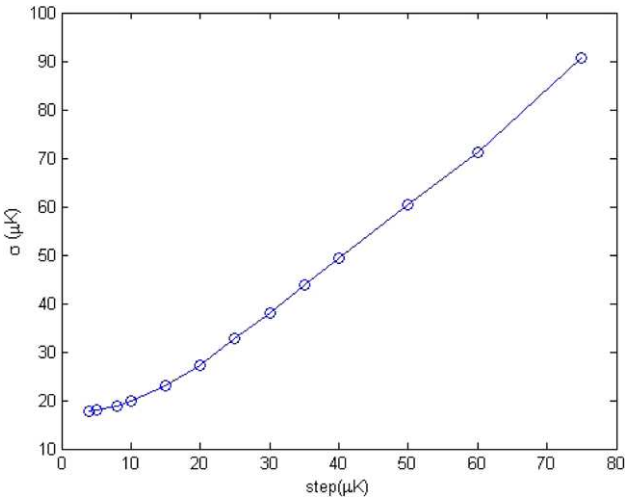

Fig. 6 Width σ of the autocorrelation versus the grid step s_T

shapes and that they can be made to overlap by a translation ΔT along the temperature axis. From the cross-correlation plot, one can estimate $\Delta T = n_{\max} \times s_T$, where $n_{\max}$ is the shift for which the cross-correlation reaches its maximum.

3.1 Grid sizing and error estimates

To choose the best size of the grid cells, we investigated the behavior of the self-correlation on a trial curve for several different choices of the steps s_T along the temperature axis. We pointed out earlier that the distribution of bins around the autocorrelation peak is Gaussian shaped. We found that the width σ of the Gaussian decreases with the grid step until it stabilizes, as shown in Fig. 6. On the basis of this behavior, a step of 15 μK in the plateau region was chosen, which is still large enough to ensure that the typical number of points in the occupied cells of the grid is five or six.

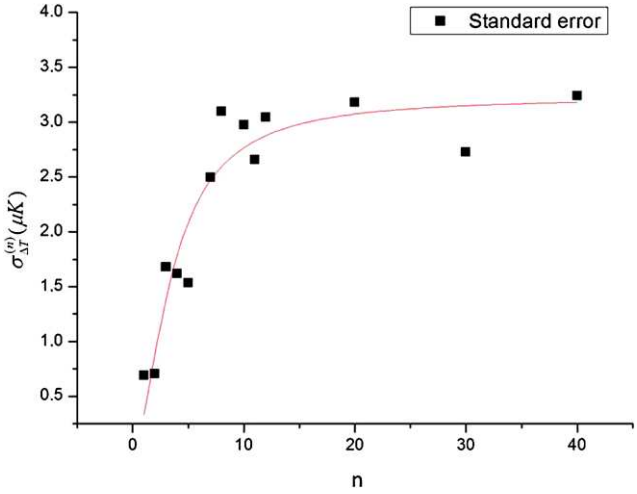

Fig. 7 The error $\sigma_{\Delta T}^{(n)}$ versus the number n of subdivisions. The error reaches a plateau for $n \approx 10$–15

The error on the temperature shifts ΔT between any two curves $R(T)$ was estimated by using the familiar jackknife method. We divided the transition region of the T–R plane into n stripes parallel to the T-axis, and of equal widths along the R-axis, and we covered each of these stripes with grids of equal steps s_T and s_R. The data points falling in each of the n stripes were then analyzed by the cross-correlation method, providing n independent estimates $\Delta T_k^{(n)}$, $k = 1, \ldots, n$ of the temperature shifts. For each number of subdivisions n, we then determined the corresponding average shift $\Delta T^{(n)} = \sum_{k=1}^{n} \frac{\Delta T_k^{(n)}}{n}$, and the variance $\sigma_{\Delta T}^{(n)} = \sqrt{\frac{\sum_{k=1}^{n} (\Delta T_k^{(n)} - \Delta T^{(n)})^2}{n-1}}$. To find the optimal number of stripes, the above process was repeated for $n \in \{1, 40\}$. In Fig. 7 we plot the behavior of $\sigma_{\Delta T}^{(n)}$ versus n. As we see, $\sigma_{\Delta T}^{(n)}$ reaches a plateau for $n \approx 10$–15, and on this basis we adopted $n = 15$ for our final assessment of the errors.

Having determined the optimal grid size and number of stripes, we could then determine the best estimates for the differences $\Delta T_c = T_c(H) - T_{c0}$ between the critical temperatures in the presence of the magnetic field and in null field, with the relative errors. For each triplet of measurements as described in Sect. 3 (see Fig. 2), we estimated

$$\Delta T_c = \Delta T_{(1,2)} - \frac{\Delta T_{(1,3)}}{2}, \tag{6}$$

where the superscripts 1 and 3 refer to the curves in zero field, and the superscript 2 to the curve in the presence of the applied field. The error on ΔT_c was taken to be

$$\sigma_{\Delta T_c} = \sqrt{\sigma_{\Delta T_{(1,2)}}^2 + \left(\frac{1}{2}\sigma_{\Delta T_{(1,3)}}\right)^2 - \mathrm{cov}_{(\Delta T_{(1,2)}, \Delta T_{(1,3)})}}, \tag{7}$$

where $\sigma_{\Delta T_{1,2}}$ and $\sigma_{\Delta T_{1,3}}$ are the standard deviations obtained as explained previously with $n = 15$.

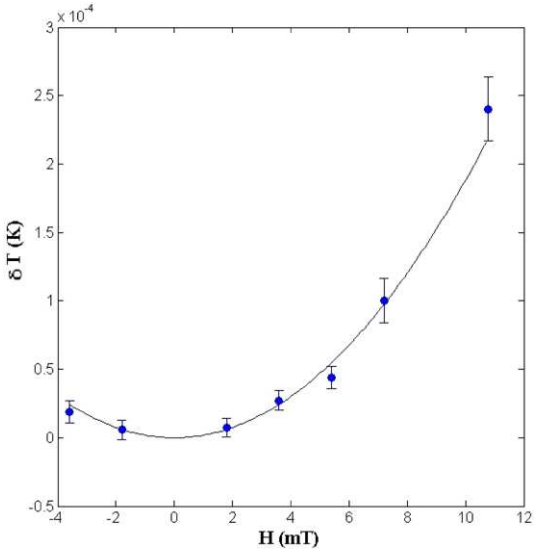

Fig. 8 Bare film data: the points follow the expected parabolic behavior

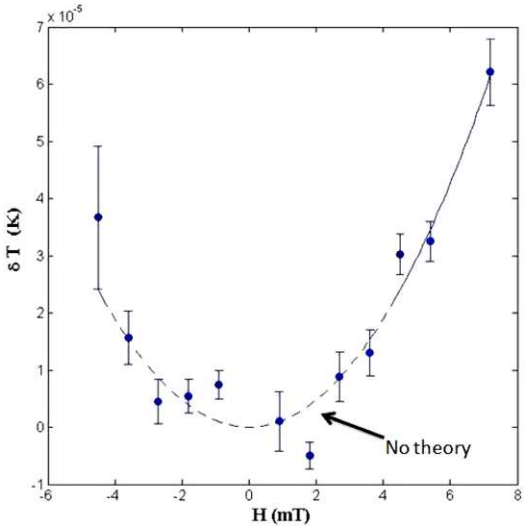

Fig. 9 In-cavity data together with a parabolic fit on higher magnetic field data: for low magnetic field, corresponding to the *dashed part* of the curve, the data do not follow the parabolic behavior

4 Experimental Results

The first thing that we checked is that the data for the bare film actually follow the theoretical law Eq. (4). According to that relation, the shifts δT should have a parabolic dependence on the applied magnetic field H. This expectation is fully verified by our data, as can be seen from Fig. 8, where the data are plotted together with a parabolic fit (continuous line).

The data for the in-cavity film are shown in Fig. 9 (note the different scales for H and δT in comparison with Fig. 8) together with a parabolic fit on higher magnetic field data. It is apparent that low-field in-cavity data show deviations from the parabolic behavior, unlike the bare-film data.

The different behavior of in-cavity data compared to bare-film data can be better appreciated from Fig. 10, where they are both plotted. It should be noted that in Fig. 10 the shifts $\delta T/T_c$ are reported as a function of the absolute value of the magnetic field; the shifts being independent of the sign of H. The two curves in Fig. 10 are the same as in Fig. 1. We observe again that the bare-film data lie nicely on the expected theoretical parabolic curve. More detailed comments are in order for the in-cavity data in Fig. 10. Let us consider first the region corresponding to $H \approx 5 \div 6$ mT: as discussed in Sect. 2, for these larger fields the Casimir energy variation is sufficiently small compared to the condensation energy to justify our perturbative calculations. In this region, one expects just a small deviation of the in-cavity data from the bare-film parabolic behavior. Unfortunately, the error bars are of the same order of magnitude of the expected small deviations and, therefore, a better sensitivity would be needed to ascertain the effect in this region. For lower

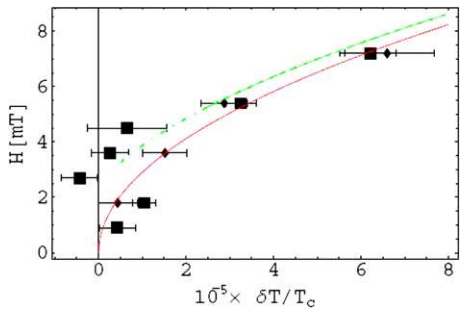

Fig. 10 Theoretical prediction and experimental results. In-cavity film data (*squares*), bare film data (*diamonds*). The *lower curve* shows the theoretical prediction for bare film data, the *upper* one that for in-cavity film data. The *point-dashed line* indicates the region where a definite theoretical prediction is not possible. Note that the point $H = 0$, $\delta T/T_c = 0$ belongs to both curves

magnetic fields, the condensation energy and the variation of Casimir energy become of the same order, the perturbation expansion is no longer possible, and deviations are possibly larger. Interestingly, in this energy region, the data of the in-cavity film are no longer compatible with a parabolic behavior, confirming and anomalous behavior with respect to the case for the bare film. We stress the fact that in this region the bare-film data lie on a parabola. This rules out the possibility that the nonparabolic behavior of the in-cavity film is due to noise. Note that, although our data had already been presented in [25], the location of points and the error bars had not been obtained with sufficient accuracy therein.

To sum up, in-cavity data show a behavior which is qualitatively different from the bare film case, and compatible with the predictions of [40, 41]. Even if we cannot draw definite conclusions from the present analysis, its results

encourage us in continuing this research. One possibility is to follow, in particular, the strategy of using very low condensation-energy materials and very low transition temperatures (see the comments following Eqs. (2, 3)).

Acknowledgements We would like to thank Professor F. Gatti and the INFN Genova group for collaboration in making the samples of Tungsten and Iridium which will be used to realize the upgrade of the experiment. G. Esposito is grateful to the Dipartimento di Scienze Fisiche of Federico II University for hospitality and support.

References

1. Casimir, H.B.G.: On the attraction between two perfectly conducting plates. Proc. K. Ned. Akad. Wet. Rev. **51**, 793 (1948)
2. Parsegian, V.A.: Van der Waals Forces. Cambridge University Press, Cambridge (2005)
3. Bordag, M., Klimchitskaya, G.L., Mohideen, U., Mostepanenko, V.M.: Advances in the Casimir Effect. Oxford University Press, Oxford (2009)
4. Elizalde, E.: Zeta function regularization in Casimir effect calculations and J.S. Dowker's contribution. Int. J. Mod. Phys. A **27**, 1260005 (2012)
5. Bimonte, G.: Johnson noise and the thermal Casimir effect. New J. Phys. **9**, 281 (2007)
6. Weinberg, S.: The cosmological constant problem. Rev. Mod. Phys. **61**, 1 (1989)
7. Feynman, R.P., Hibbs, A.R.: Quantum Mechanics and Path Integrals, pp. 244–246. McGraw-Hill, New York (1965)
8. Brown, L.S., Maclay, G.J.: Vacuum stress between conducting plates: an image solution. Phys. Rev. **184**, 1272 (1969)
9. Sciama, D.W.: In: Saunders, S., Brown, H.R. (eds.) The Philosophy of Vacuum, p. 137. Clarendon, Oxford (1991)
10. Fulling, S.A., Milton, K.A., Parashar, P., Romeo, A., Shajesh, K.V., Wagner, J.: How does Casimir energy fall? Phys. Rev. D **76**, 025004 (2007)
11. Milton, K.A., Parashar, P., Shajesh, K.V., Wagner, J.: How does Casimir energy fall? II. Gravitational acceleration of quantum vacuum energy. J. Phys. A **40**, 10935 (2007)
12. Milton, K.A., Fulling, S.A., Parashar, P., Romeo, A., Shajesh, K.V., Wagner, J.A.: Gravitational and inertial mass of Casimir energy. J. Phys. A **41**, 164052 (2008)
13. Shajesh, K.V., Milton, K.A., Parashar, P., Wagner, J.A.: How does Casimir energy fall? III. Inertial forces on vacuum energy. J. Phys. A **41**, 164058 (2008)
14. Estrada, R., Fulling, S.A., Liu, Z., Kaplan, L., Kirsten, K., Milton, K.A.: Vacuum stress–energy density and its gravitational implications. J. Phys. A **41**, 164055 (2008)
15. Milton, K.A., Parashar, P., Wagner, J., Shajesh, K.V., Romeo, A., Fulling, S.: How does quantum vacuum energy accelerate? arXiv:0810.0081 [hep-th]
16. Milton, K.A.: Local and global Casimir energies: divergences, renormalization, and the coupling to gravity. Lect. Notes Phys. **834**, 39 (2011)
17. Calloni, E., Di Fiore, L., Esposito, G., Milano, L., Rosa, L.: Vacuum fluctuation force on a rigid Casimir cavity in a gravitational field. Phys. Lett. A **297**, 328 (2002)
18. Sathyaprakash, B., Abernathy, M., Acernese, F., Andersson, P.A.-S.N., Arun, K., Barone, F., et al.: Class. Quantum Gravity **29**, 124013 (2012)
19. Abadie, J., Abbott, B.P., Abbott, R., et al.: Phys. Rev. D **85**, 022001 (2012)
20. Calloni, E., Di Fiore, L., Esposito, G., Milano, L., Rosa, L.: Gravitational effects on a rigid Casimir cavity. Int. J. Mod. Phys. A **17**, 804 (2002)
21. Bimonte, G., Calloni, E., Esposito, G., Rosa, L.: Energy-momentum tensor for a Casimir apparatus in a weak gravitational field. Phys. Rev. D **74**, 085011 (2006); erratum Phys. Rev. D **75**, 049904 (2007); erratum Phys. Rev. D **75**, 089901 (2007); erratum Phys. Rev. D **77**, 109903 (2008)
22. Bimonte, G., Calloni, E., Esposito, G., Rosa, L.: Relativistic mechanics of Casimir apparatuses in a weak gravitational field. Phys. Rev. D **76**, 025008 (2007)
23. Chen, F., Klimchitskaya, G.L., Mostepanenko, V.M., Mohideen, U.: Demonstration of optically modulated dispersion forces. Opt. Express **15**, 4823 (2007)
24. Chen, F., Klimchitskaya, G.L., Mostepanenko, V.M., Mohideen, U.: Control of the Casimir force by the modification of dielectric properties with light. Phys. Rev. B **76**, 035338 (2007)
25. Bimonte, G., Born, D., Calloni, E., Esposito, G., Huebner, U., Il'ichev, E., Rosa, L., Tafuri, F., Vaglio, R.: Low noise cryogenic system for the measurement of the Casimir energy in rigid cavities. J. Phys. A **41**, 164023 (2008)
26. Tafuri, F., Kirtley, J.R., Born, D., Stornaiuolo, D., Medaglia, P.G., Orgiani, P., Balestrino, G., Kogan, V.G.: Dissipation in ultra-thin current-carrying superconducting bridges; evidence for quantum tunneling of Pearl vortices. Europhys. Lett. **73**, 948 (2006)
27. Fittipaldi, R., Vecchione, A., Ciancio, R., Pace, S., Cuoco, M., Stornaiuolo, D., Born, D., Tafuri, F., Olsson, E., Kittaka, S., Yaguchi, H., Maeno, Y.: Superconductivity in Sr(2)RuO(4)-Sr(3)Ru(2)O(7) eutectic crystals. Europhys. Lett. **83**, 27007 (2008)
28. Carillo, F., Papari, G., Stornaiuolo, D., Born, D., Montemurro, D., Pingue, P., Beltram, F., Tafuri, F.: Little-Parks effect in single YBaCuO sub-micron ring. Phys. Rev. B **81**, 054505 (2010)
29. Stornaiuolo, D., Rotoli, G., Cedergren, K., Born, D., Bauch, T., Lombardi, F., Tafuri, F.: Submicron YBaCuO biepitaxial Josephson junctions: d-wave effects and phase dynamics. J. Appl. Phys. **107**, 113901 (2010)
30. Stornaiuolo, D., Papari, G., Cennamo, N., Carillo, F., Longobardi, L., Massarotti, D., Barone, A., Tafuri, F.: High quality factor HTS Josephson junctions on low loss substrates. Supercond. Sci. Technol., **24**, 045008 (2011)
31. Longobardi, L., Massarotti, D., Stornaiuolo, D., Galletti, L., Rotoli, G., Lombardi, F., Tafuri, F.: Direct transition from quantum escape to phase diffusion regime in YBaCuO biepitaxial Josephson junctions. Phys. Rev. Lett. **109**, 050601 (2012)
32. Longobardi, L., Massarotti, D., Rotoli, G., Stornaiuolo, D., Papari, G., Kawakami, A., Pepe, G.P., Barone, A., Tafuri, F.: Thermal hopping and retrapping of a Brownian particle in the tilted periodic potential of a NbN/MgO/NbN Josephson junction. Phys. Rev. B **84**, 184504 (2011)
33. Kirtley, J.R., Tsuei, C.C., Tafuri, F.: Evidence for thermally activated spontaneous fluxoid formation in superconducting thin-film rings. Phys. Rev. Lett. **90**, 257001 (2003)
34. Carillo, F., Papari, G., Stornaiuolo, D., Born, D., Montemurro, D., Pingue, P., Beltram, F., Tafuri, F.: Phys. Rev. B **81**, 054505 (2010)
35. Stornaiuolo, D., Rotoli, G., Cedergren, K., Born, D., Bauch, T., Lombardi, F., Tafuri, F.: J. Appl. Phys. **107**, 113901 (2010)
36. Stornaiuolo, D., Papari, G., Cennamo, N., Carillo, F., Longobardi, L., Massarotti, D., Barone, A., Tafuri, F.: Supercond. Sci. Technol. **24**, 045008 (2011)
37. Rotoli, G., Bauch, T., Lindstrom, T., Stornaiuolo, D., Tafuri, F., Lombardi, F.: Classical resonant activation of a Josephson junction embedded in an LC-circuit. Phys. Rev. B **75**, 144501 (2007)
38. Di Capua, R., Aebersold, H.U., Ferdeghini, C., Ferrando, V., Orgiani, P., Putti, M., Salluzzo, M., Vaglio, R., Xi, X.X.: Role of

interband scattering in neutron irradiated MgB_2 thin films by scanning tunneling spectroscopy measurements. Phys. Rev. B **75**, 014515 (2007)
39. Salluzzo, M., Ghiringhelli, G., Cezar, J.C., Brookes, N.B., De Luca, G.M., Fracassi, F., Vaglio, R.: Indirect electric field doping of the CuO_2 planes of the cuprate $NdBa_2Cu_3O_7$ superconductor. Phys. Rev. Lett. **100**, 056810 (2008)
40. Bimonte, G., Calloni, E., Esposito, G., Milano, L., Rosa, L.: Towards measuring variations of Casimir energy by a superconducting cavity. Phys. Rev. Lett. **94**, 180402 (2005)
41. Bimonte, G., Calloni, E., Esposito, G., Rosa, L.: Variations of Casimir energy from a superconducting transition. Nucl. Phys. B **726**, 441 (2005)
42. Glover, R.E. III, Tinkham, M.: Conductivity of superconducting films for photon energies between 0.3 and 40 kTc. Phys. Rev. **108**, 243 (1957)
43. Bimonte, G.: Casimir effect in a superconducting cavity and the thermal controversy. Phys. Rev. A **78**, 062101 (2008)
44. Bimonte, G., Haakh, H., Henkel, C., Intravaia, F.: Optical BCS conductivity at imaginary frequencies and dispersion energies of superconductors. J. Phys. A **43**, 145304 (2010)
45. Tinkham, M.: Introduction to Superconductivity. McGraw-Hill, New York (1975)
46. Lewis, H.W.: Superconductivity and electronic specific heat. Phys. Rev. **101**, 939 (1956)